Journal of Statistical Modelling: Theory and Applications
Vol. 6, No. 1, 2025, pp. 115-131
Yazd University Press 2025

JSMTA

Research Paper

Color image denoising using a hybrid algorithm based on singular spectrum analysis and principal component analysis methods

Masoud Yarmohammadi*, Mohammad Shourvazi, Parviz Nasiri
Department of Statistics, University of Payame Noor, Tehran, Iran

Received: September 22, 2025/ Revised: December 02, 2025/ Accepted: December 27, 2025

Abstract: In this paper, a hybrid algorithm based on singular spectrum analysis and principal component analysis is proposed for denoising color images. The main novelty of this approach lies in the simultaneous utilization of singular spectrum analysis's capability to separate signal and noise in the time-series domain, along with principal component analysis's ability to remove correlations among the red, green, and blue channels of color images. To validate the effectiveness of the proposed method, peak signal-to-noise ratio and structural similarity index are employed on reference images that are contaminated with random noise at different levels. The experimental results indicate that the proposed algorithm achieves superior performance, particularly at higher noise levels. Specifically, the results demonstrate higher peak signal-to-noise ratio and structural similarity values when compared with principal component analysis-based bootstrapping methods and eigenvalue-based denoising approaches.

Keywords: Denoising color images; Peak signal-to-noise ratio; Principal component analysis; Singular spectrum analysis; Structural similarity.
Mathematics Subject Classification (2010): 62M10, 62H25, 94A08.

1 Introduction

Noise is one of the fundamental challenges in image processing, particularly in medical and satellite imaging. It can severely degrade image quality and consequently reduce the accuracy of diagnosis and subsequent analyses. Shakeri et al. (2019) demonstrated

*Corresponding author: masyar@pnu.ac.ir

that multiscale noise in magnetic resonance imaging (MRI), caused by hardware limitations, reduces the detection of small lesions by up to 40%. In satellite images, atmospheric noise such as cloud cover or dust storms decreases land cover classification accuracy by approximately 25%. Similarly, in medical images such as ultrasound, radiography, and MRI the presence of noise can obscure abnormalities and hinder reliable diagnosis. In satellite imaging, noise may lead to misinterpretation of data and inaccurate geographic analysis, which are critical in urban planning and natural resource management (Moreno López et al., 2021).

Conventional denoising methods often face limitations in preserving structural details or maintaining robustness against noise. Yang et al. (2022) reported that traditional approaches to noise removal tend to reduce image quality under specific conditions. Likewise, according to Zhang et al. (2023), classical methods such as median or Gaussian filtering may fail when confronted with complex noise structures. Recent studies have proposed advanced dictionary learning-based methods for image denoising. For instance, an improved K-singular value decomposition (K-SVD) algorithm with atom optimization has been developed to enhance noise removal while preserving structural details (Chen et al., 2022). In this approach, a sparse representation of image patches is obtained via a refined dictionary, followed by elimination of dictionary atoms that primarily model noise. Additionally, non-local self-similarity (NSS) priors are incorporated to maintain textures and edges. This method demonstrated superior performance over classical techniques such as median filtering, BM3D, and standard K-SVD, especially under strong Gaussian noise conditions.

In this study, we focus specifically on additive Gaussian noise in RGB color images. Existing denoising techniques typically include mean filters, Gaussian filters, median filters, transform-based approaches, and nonlinear algorithms. However, these methods often involve trade-offs between noise suppression and the preservation of fine structural details, thereby motivating the development of more advanced and hybrid denoising frameworks (Mafi et al., 2019).

In digital imaging, a standard color image is constituted by three distinct matrices, each corresponding to one of the primary color channels: Red (R), Green (G), and Blue (B). The dimensions of these matrices are determined by the spatial resolution of the image, meaning their height and width equal the number of pixels along the image's vertical and horizontal axes, respectively (Ghasemi, 2023). Each pixel within a color image is thus represented by a triplet of intensity values for the respective channels. Conventionally, each intensity value is encoded as an 8-bit integer, constraining its range to integers between 0 and 255. Consequently, any color image can be mathematically represented as three matrices populated with values in this range. This three-matrix representation is a foundational, standard, and computationally efficient model in digital image processing (Ghasemi and Safariyan, 2024).

A significant challenge in processing color images arises from the inherent spectral correlation among the three-color channels, which introduces considerable computational complexity in tasks such as color image denoising. Ignoring these inter-channel dependencies can lead to suboptimal results. Therefore, the scientific gap addressed in this study is twofold: first, the inadequacy of prior research in explicitly modeling the dependencies between the color channels; and second, the need to develop a denoising framework that effectively accounts for these correlations, providing a robust and re-

liable approach to improve image quality. To bridge this gap, this research proposes a hybrid singular spectrum analysis–principal component analysis (SSA–PCA) denoising framework enriched with an exponential weighted averaging (EWA) strategy. The proposed model leverages the multi-scale decomposition capability of SSA alongside the dimensionality-reduction and correlation-capturing power of PCA, enabling a joint treatment of structural and spectral information in RGB images. The introduction of EWA as an adaptive weighting mechanism constitutes a key methodological contribution, offering optimization-oriented weights that have not been explored in previous SSA-based denoising frameworks, particularly for color images with inter-channel correlations. By integrating SSA, PCA, and EWA within a unified structure, the proposed method aims to achieve superior noise suppression while preserving fine textures and maintaining chromatic consistency across the RGB channels.

The rest of this paper is organized as follows. Section 2 introduces SSA and the EWA enhancement. Section 3 discusses the application of SSA to color image denoising. Section 4 describes the evaluation metrics and criteria for the proposed model. Section 5 presents theoretical Foundations and step-by-step methodology of the proposed hybrid SSA-PCA model. Section 6 presents the experimental results of the proposed algorithm. The discussion and conclusions are presented in Section 7.

2 Singular spectrum analysis

Singular spectrum analysis is a relatively modern and powerful method in the field of time series analysis. As a non-parametric technique, its unique characteristics, such as not requiring the assumptions of stationarity or normality of residuals, have attracted significant attention from researchers in time series analysis and econometrics, leading to its increasingly widespread application. In the SSA method, a time series is decomposed into its constituent components, such as trend, seasonal components with different periodicities, and noise. Following this decomposition and the removal of noise from the series, the components are reconstructed. Finally, using forecasting methods developed within the SSA framework, predictions about the future of the time series are made (Golyandina and Korobeynikov, 2014).

The SSA method consists of four main stages, categorized into two broad sections: *Decomposition* and *Reconstruction*. The decomposition section itself comprises two steps: (1) Embedding and (2) SVD. The reconstruction section also includes two steps: (1) Grouping and (2) Diagonal Averaging.

Suppose

$$X_N = \{x_1, x_2, \ldots, x_N\},$$

is an observed time series of length N. Furthermore, consider a positive integer L, referred to as the window length, such that $1 < L < N$. In the embedding step, the time series is transformed into $K = N - L + 1$ lagged vectors (sub-series). The i-th lagged vector, for $i = 1, 2, \ldots, K$, is defined as

$$X_i = (x_i, x_{i+1}, \ldots, x_{i+L-1})^T.$$

Consequently, the trajectory matrix X is constructed as

$$X = [X_1, X_2, \ldots, X_K] = (x_{ij})_{i,j=1}^{L,K}, \tag{1}$$

that is,

$$X = \begin{bmatrix} x_1 & x_2 & \cdots & x_K \\ x_2 & x_3 & \cdots & x_{K+1} \\ \vdots & \vdots & \ddots & \vdots \\ x_L & x_{L+1} & \cdots & x_N \end{bmatrix}.$$

In the second step of the decomposition, the SVD of the trajectory matrix is computed. Assume that $\lambda_1, \lambda_2, \ldots, \lambda_L$, are the eigenvalues of the matrix XX^T (also referred to as the covariance matrix in this context), sorted in descending order of magnitude such that $\lambda_1 > \lambda_2 > \cdots > \lambda_L \geq 0$. Let $U_1, U_2, \ldots, U_L$ denote the corresponding orthonormal eigenvectors (i.e., the principal components). Then, the SVD of the trajectory matrix X can be expressed as

$$X = X_1 + \cdots + X_d = \sum_{i=1}^{d} \sqrt{\lambda_i}\, U_i V_i^T, \tag{2}$$

where $d = \operatorname{rank}(X)$ is the rank of the trajectory matrix, and

$$V_i = \frac{X^T U_i}{\sqrt{\lambda_i}}.$$

The triple $(\sqrt{\lambda_i}, U_i, V_i^T)$ is referred to as an *eigentriple*. Here, $\sqrt{\lambda_i}$ is the i-th singular value, and the set $\{\sqrt{\lambda_1}, \ldots, \sqrt{\lambda_L}\}$, is termed the singular spectrum.

The objective of the third step, *Grouping*, is to identify and cluster the eigentriples corresponding to distinct components of the original time series, such as trend, oscillatory (seasonal) patterns, and noise. Let the set of all eigentriples obtained from the SVD be $\{(\sqrt{\lambda_i}, U_i, V_i^T)\}_{i=1}^{d}$. The grouping procedure partitions the index set $\{1, 2, \ldots, d\}$ into m disjoint subsets $I_1, I_2, \ldots, I_m$ such that each subset I_j corresponds to one meaningful component of the time series. Mathematically, the grouped matrix for the j-th component is defined as:

$$X_{I_j} = \sum_{i \in I_j} \sqrt{\lambda_i}\, U_i V_i^T, \quad j = 1, \ldots, m.$$

The selection of eigentriples into each group is typically guided by the analysis of singular values (e.g., scree plot), eigenvectors (principal components), and pairwise correlations of eigenvectors. In practice, components with slowly decaying singular values often represent the trend, while oscillatory eigenvectors with similar singular values capture periodic or quasi-periodic signals, and remaining small-magnitude eigentriples are associated with noise.

The fourth and final step, *Diagonal Averaging* (also called Hankelization), converts each grouped matrix $X_{I_j} \in \mathbb{R}^{L \times K}$ back into a time series of length N. Denote the reconstructed time series corresponding to the j-th group as $\widetilde{X}_N^{(j)} = \{\tilde{x}_1^{(j)}, \tilde{x}_2^{(j)}, \ldots, \tilde{x}_N^{(j)}\}$. The diagonal averaging operation is defined as

$$\tilde{x}_k^{(j)} = \begin{cases} \frac{1}{k} \sum_{i=1}^{k} x_{i,k-i+1}^{(j)}, & 1 \leq k < L, \\ \frac{1}{L} \sum_{i=1}^{L} x_{i,k-i+1}^{(j)}, & L \leq k \leq K, \\ \frac{1}{N-k+1} \sum_{i=k-K+1}^{L} x_{i,k-i+1}^{(j)}, & K < k \leq N, \end{cases}$$

where $x_{i,j}^{(j)}$ are the entries of X_{I_j}. This averaging along the anti-diagonals ensures that the reconstructed matrix is Hankel (all elements along each diagonal are equal), yielding a one-dimensional time series. After applying diagonal averaging to all m groups, the final reconstructed series is obtained as

$$\widetilde{X}_N = \sum_{j=1}^{m} \widetilde{X}_N^{(j)},$$

where the contribution of each component can be analyzed separately or used for further processing, such as denoising, forecasting, or feature extraction (Golyandina et al., 2018).

2.1 Exponential weighted averaging for enhanced SSA

In the theory of SSA, the process of Hankelization plays a central role in signal reconstruction. According to the Theorem of Optimal Diagonal Averaging, the unique Hankel matrix that minimizes the Frobenius norm distance from a given matrix is obtained by taking the arithmetic mean along the anti-diagonals (Golyandina et al., 2001). This establishes the arithmetic mean as the mathematically optimal choice for Hankelization.

Building on this foundation, researchers have sought to improve averaging-based filters in image processing. One of the earliest attempts was made by Momot et al. (2005), who introduced Bayesian weighted averaging for two-dimensional image filtering. Originally designed for noise reduction in electrocardiographic signals, this method was shown to outperform arithmetic mean and median filters in biomedical image denoising. More recently, Wang et al. (2023) proposed a novel weighted averaging filter based on the Atangana-Baleanu fractional integral operator to address salt-and-pepper noise. Their method, which employs symmetric window mask structures and an iterative scheme for handling high-density noise, demonstrated superior performance in terms of peak signal-to-noise ratio (PSNR) and structural similarity (SSIM), while also ensuring computational efficiency and preservation of image details.

Although diagonal averaging is mathematically justified as the optimal procedure in the sense of minimizing the Frobenius norm distance, its practical limitations, such as sensitivity to noise and the blurring of fine structural details, highlight the need for more robust alternatives. Motivated by these shortcomings, this study employs EWA in place of simple anti-diagonal averaging in the reconstruction stage of SSA. By assigning larger weights to elements that are spatially or temporally closer to the reconstruction point and gradually decreasing the weights of more distant elements, EWA effectively suppresses random noise while preserving the dominant structures of the signal or image. Consequently, the method not only improves noise reduction but also enables more accurate reconstruction of fine-scale details. Furthermore, the presence of a decay parameter in EWA introduces flexibility, allowing for a tunable balance between noise suppression and detail preservation, and thereby ensuring adaptability to various noise levels and structural complexities of the data. This approach is applicable to each channel of color images (RGB), either independently or considering inter-channel correlations, making it suitable for SSA–PCA-based denoising frameworks.

In the reconstruction stage of SSA, instead of using the simple average along the anti-diagonals of the Hankel matrix, an EWA is applied. Let the reconstructed matrix be $X \in \mathbb{R}^{L\times K}$. The reconstructed signal at time position t is defined as

$$x(t) = \frac{\sum_{i+j-1=t} \omega_{i,j}\, X_{i,j}}{\sum_{i+j-1=t} \omega_{i,j}}, \quad t = 1, 2, \ldots, N. \tag{3}$$

where the weights are given by an exponential function depending on the distance from the center

$$\omega_{i,j} = \exp(-\alpha|t - c|), \quad c = \frac{N+1}{2}, \quad \alpha \approx 0.05. \tag{4}$$

Here, $t = i+j-1$ is the time index corresponding to element $X_{i,j}$, c is the center of the reconstructed signal, and $\alpha > 0$ is the decay parameter that controls the contribution of elements based on their distance from the center. If $\alpha \to 0$, the exponential weighted average reduces to the simple diagonal averaging used in classical SSA. For larger α, elements closer to the center dominate the reconstruction. This approach emphasizes the central structure of the signal, leading to improved denoising performance while preserving the main patterns.

3 Color image denoising based on SSA

Rodríguez-Aragon and Zhigljavsky (2010), in their seminal research titled "Singular Spectrum Analysis for Image Processing," utilized a two-dimensional extension of SSA, termed 2D-SSA, for image denoising. In this methodology, local patches are extracted from the image. Noise is then removed by applying the SVD to these patches, followed by their reconstruction.

A digital image is fundamentally represented as a matrix of intensity or color values. In single-channel grayscale images, each matrix element represents a pixel's brightness level. In contrast, color images are typically represented by three such matrices, each corresponding to the Red, Green, and Blue (RGB) color channels (Saeedi-Zarandi, 2021). Crucially, this approach did not account for the inherent correlation between the three image channels; each matrix (R, G, B) was decomposed and denoised separately. This omission is significant, as numerous studies have established that substantial correlation exists between the red, green, and blue color channels (Ghasemi et al., 2022).

While SSA has gained traction in recent years for its proven ability to effectively separate noise components from non-linear signals, its application in image processing is not without limitations. For instance, studies such as Zou et al. (2023) have highlighted a key limitation of SSA: its tendency to over-smooth fine details and edges, particularly in ultrasound images. Furthermore, processing the channels independently leads to a lack of coordinated spectral processing, often resulting in color artifacts and inconsistencies in the final output. This disjointed approach fails to exploit the inter-channel correlations, potentially introducing distortions and suboptimal denoising performance in color images.

Li and Wu (2025) proposed a novel hybrid-domain synergistic transformer framework, termed HDST, for hyperspectral image denoising. Unlike conventional ap-

proaches that focus on either spatial or spectral features, their method simultaneously exploits spatial, spectral, and frequency domains to better capture the inherent correlations in hyperspectral data. The framework integrates a frequency-domain preprocessing module using fast Fourier transform (FFT) with multi-band convolution to separate noise components, followed by a cross-domain attention mechanism that adaptively fuses spatial textures with frequency priors. Moreover, the hierarchical network design allows shallow layers to address large-scale noise statistics, while deeper layers concentrate on restoring fine structural details. Experimental results on both real and synthetic datasets demonstrated that HDST achieves superior denoising performance compared to existing techniques, while maintaining computational efficiency.

In many denoising scenarios, the decision to preserve or remove a pixel's value inherently involves a degree of uncertainty. Addressing this, Ghasemi and Yousefinejad (2025) argued that Fuzzy Logic provides a framework for continuous, non-binary decision-making. Consequently, a hybrid denoising strategy that synergistically combines the strengths of multiple methods has the potential to significantly improve performance metrics for image denoising.

Therefore, the proposed model of the present research aims to enhance denoising performance for color images by integrating SSA with PCA. This hybrid approach is specifically designed to model the dependencies between color channels and leverage the multi-dimensional information within the image. In other words, to effectively address the challenge of reducing inter-channel correlation in the three-color matrices, the proposed framework of this study should be adopted. In summary, this research seeks to develop a statistical modeling framework based on SSA and complementary techniques such as exponentially weighted averaging and the optimization of key parameters (the window length L and the reconstruction rank r in SSA) to significantly increase the efficacy of the color image denoising process.

4 Evaluation of the proposed model

In order to objectively evaluate the performance of the proposed model in enhancing image quality and reducing noise, it is necessary to utilize standard and reliable metrics. This study employs two widely used and conventional criteria:

Peak Signal-to-Noise Ratio (PSNR): This metric is calculated based on the Mean Squared Error (MSE) and represents the ratio between the maximum possible power of the signal and the power of corrupting noise. A higher PSNR value indicates superior image quality. The PSNR is defined as follows

$$\mathrm{PSNR} = 10 \cdot \log_{10} \left(\frac{\mathrm{MAX}^2}{\mathrm{MSE}} \right), \tag{5}$$

where MAX is the maximum achievable value in the input image data type (e.g., 255 for 8-bit images), and MSE represents the Mean Squared Error between the original and denoised images (Moreno López et al., 2021).

Structural Similarity Index (SSIM): This index measures the structural similarity between the denoised image and the original reference image. It is defined within

the range $[-1, 1]$, where a value closer to 1 indicates a high degree of structural similarity. The SSIM is a perceptual metric that incorporates comparisons of luminance, contrast, and structure. It is computed as

$$\mathrm{SSIM} = \frac{(2\mu_x\mu_y + C_1)(2\sigma_{xy} + C_2)}{(\mu_x^2 + \mu_y^2 + C_1)(\sigma_x^2 + \sigma_y^2 + C_2)}, \tag{6}$$

where

- μ_x and μ_y are the local means of the reference and the distorted image patches, respectively,
- σ_x^2 and σ_y^2 represent the variances of the reference and the distorted image patches, respectively,
- σ_{xy} denotes the covariance between the reference and distorted patches,
- C_1 and C_2 are constants included to avoid division by zero and ensure numerical stability. In this paper, their values are determined following the approach of Peng et al. (2020).

These metrics provide a comprehensive assessment of both pixel-level accuracy (PSNR) and perceptual quality (SSIM), ensuring a robust evaluation of the denoising performance (Horé and Ziou, 2010).

5 Theoretical foundations and methodology of the SSA–PCA framework

To effectively address the problem of color image denoising in the presence of mixed noise, this study integrates PCA and SSA within a unified framework. The methodology is designed to exploit both local spatial information and spectral correlations across RGB channels, ensuring that noise components are attenuated without compromising the fine structural details of the image.

The process begins by constructing local windows around each pixel to capture neighborhood information and applying PCA for dimensionality reduction, which separates the dominant structural components from noise-dominated directions. Subsequently, SSA is employed on the reconstructed local signals, where the Hankel matrix formulation and low-rank approximation enable the extraction of essential signal patterns. To further improve reconstruction accuracy, exponential weighted diagonal averaging is introduced, enhancing the contribution of significant components while suppressing residual noise. This multi-stage approach provides a balance between computational efficiency, structural preservation, and denoising performance. The following section first presents the theoretical background for determining the patch size (Δ) and the number of significant principal components in PCA. Subsequently, the theoretical basis for EWA is discussed. Finally, the step-by-step implementation of the algorithm in MATLAB is provided.

5.1 Theoretical background

Let $\mathcal{I} \in \mathbb{R}^{M\times N\times 3}$ be a clean RGB image, and let

$$\mathcal{Y} = \mathcal{I} + \mathcal{E},$$

be the observed noisy version, where $\mathcal{E}$ consists of Additive Gaussian Noise (AGN or AWGN). In patch-based image denoising methods, the choice of the local patch size, denoted by Δ, plays a critical role in the performance of the filter. A small initial patch size, typically $\Delta = 1$ corresponding to a 3×3 window, is chosen as a starting point. This size is large enough to compute meaningful local statistics, such as variance, around the central pixel, while keeping the computational cost low. Starting from this minimal patch, the algorithm allows for *adaptive patch sizing*, where Δ can increase in smooth or highly noisy regions, and remain small in textured areas to preserve fine details Monagi and El-Sakka (2017); Buades et al. (2005); Dabov et al. (2007). This approach is consistent with state-of-the-art patch-based methods, which show that adaptive patch selection improves denoising performance across various noise levels Monagi and El-Sakka (2017).

Similarly, the length of the SSA window, L, is chosen adaptively based on the size of the patch and the local variance. The window must be large enough to capture the main local signal trend but not so large as to oversmooth fine image structures. In the proposed algorithm, L is set as a fraction of the total number of pixels in the patch, allowing the SSA filtering to adjust automatically according to the local content, which ensures an optimal trade-off between noise suppression and detail preservation.

For the determination of the effective number of principal components r in the PCA step, the method of *Singular Value Hard Thresholding (SVHT)* proposed by Donoho and Gavish Donoho and Gavish (2014) is used. Let $X \in \mathbb{R}^{m\times n}$ denote a patch matrix corrupted by additive Gaussian noise with variance σ^2. The SVD of X is given by

$$X = U\,\mathrm{diag}(\sigma_1, \sigma_2, \ldots, \sigma_p)\,V^\top, \quad p = \min(m, n),$$

where σ_i are the singular values. The number of significant principal components r is determined via hard thresholding

$$r = \sum_{i=1}^{p} \mathbf{1}\big(\sigma_i > \tau^*\big), \qquad \tau^* = \omega(\beta)\cdot \mathrm{median}(\sigma_i), \qquad \beta = \frac{\min(m,n)}{\max(m,n)},$$

and $\mathbf{1}(\cdot)$ is the indicator function, and $\omega(\beta)$ is the optimal scaling factor defined as

$$\omega(\beta) = \begin{cases} 2.858, & \beta \le 0.01, \\ \sqrt{2(\beta+1) + \frac{8\beta}{(\beta+1)+\sqrt{\beta^2+14\beta+1}}}, & \beta > 0.01. \end{cases}$$

The reconstructed patch using the first r principal components is $\hat{X} = (X-\mu)\,V_r\,V_r^\top + \mu$, where $\mu = \mathrm{mean}(X)$ and $V_r \in \mathbb{R}^{n\times r}$ contains the first r right singular vectors. This approach ensures that only the components related to the main signal are retained, while components dominated by noise are discarded, providing an adaptive and theoretically justified selection of PCA components. It is demonstrated that EWA is a principled generalization of classical diagonal averaging, derived as the unique minimizer of a weighted Frobenius projection onto the Hankel manifold and formally presented through a Bayesian heteroscedastic noise model. Classical SSA reconstructs the signal using *uniform* diagonal averaging, which solves $\min_{H\in\mathcal{H}} \|X - H\|_F$. To generalize this, define the weighted Frobenius norm

$$\|A\|_W^2 = \sum_{i,j} \omega_{i,j} A_{i,j}^2, \quad \omega_{i,j} > 0.$$

The unique Hankel matrix minimizing $\min_{H\in\mathcal{H}} \|X-H\|_W^2$, is obtained via weighted anti-diagonal averaging $h_t^\star = \frac{\sum_{i+j-1=t}\omega_{i,j}X_{i,j}}{\sum_{i+j-1=t}\omega_{i,j}}$, $t=1,\ldots,L+K-1$. Choosing exponential weights

$$\omega_{i,j} = \exp(-\alpha|(i+j-1)-c|), \quad c=\frac{L+K}{2}, \quad \alpha>0,$$

yields the EWA formulation.

For $\alpha\to 0$, classical SSA is recovered, noise-dominated contributions. with Bayesian approach; If $X_{i,j}=h(t)+\varepsilon_{i,j}$, $\varepsilon_{i,j}\sim\mathcal{N}(0,\sigma_{i,j}^2)$, and noise variance increases with distance from the center, $\sigma_{i,j}^2\propto e^{\alpha|t-c|}$, the MAP estimator of $h(t)$ is exactly the EWA formula. Thus, EWA has both optimization-based and Bayesian optimality interpretations.

Implications for SSA Reconstruction. By integrating exponential weighting into the Hankelization step, the proposed method:
• reduces the influence of distant and potentially noisy elements,
• preserves fine-scale structures that tend to be blurred by uniform averaging,
• enhances the robustness of SSA to high noise levels,
• provides a tunable balance between noise suppression and detail preservation via the decay parameter α.
Consequently, the reconstruction process becomes more adaptive to the underlying signal characteristics and achieves superior denoising performance while maintaining computational efficiency.

5.2 Step-by-step methodology

The following steps summarize the complete procedure employed in this study:
1. **Image Loading:** The original image and its noisy counterpart were loaded, where the noise level was artificially introduced at 10%, 20%, and 30%.
2. **Initial Control Parameters:** The initial local window size Δ_0, the SSA window-length ratio L_{percent}, and the noise-detection threshold α_{Thr} were initialized. Unlike fixed-size frameworks, the proposed method dynamically adjusts Δ during processing based on local statistics.
3. **Adaptive Local Window Selection:** For each pixel (excluding boundary margins), an initial $(1+2\Delta_0)\times(1+2\Delta_0)$ patch was extracted. The variance of this initial patch was computed, and the patch size was adaptively updated using

$$\Delta = \max\left(1,\ \text{round}\left(\Delta_0\left[1+\frac{\text{median}(\boldsymbol{x})}{\text{Var}(\boldsymbol{x})}\right]\right)\right),$$

where $\boldsymbol{x}$ denotes the vectorized pixel intensities of the initial patch. Smooth regions thus receive larger patches (stronger denoising), while textured regions receive smaller patches (better detail preservation).
4. **Noise Detection Prior to Processing:** Before performing PCA or SSA, the variance of the adaptively sized patch was compared with a data-dependent threshold:

$$\text{Var}(\boldsymbol{x}) > \alpha_{\text{Thr}}\cdot\text{median}(\boldsymbol{x}).$$

Only patches satisfying this criterion undergo PCA–SSA processing; otherwise, the center pixel is left unchanged. This substantially reduces unnecessary computations in smooth, low-noise areas.
5. **Local PCA with Automatic Component Selection:**
(a) The patch pixels from all RGB channels were rearranged into a matrix and mean-centered.
(b) SVD was applied.
(c) The optimal number of principal components r was determined automatically using the Donoho–Gavish universal threshold:

$$r = \#\{\, \sigma_i > \tau \,\},$$

where σ_i are singular values and $\tau = \omega(\beta) \cdot \text{median}(\sigma_i)$ is the optimal hard threshold.
(d) The patch was reconstructed using the first r principal components.

This adaptive selection of r replaces fixed-component heuristics used in conventional PCA denoising.
6. **SSA:** For each channel of the PCA-reconstructed patch, a 1D SSA model was applied. The embedding dimension was chosen as

$$L = \max(2,\ \text{round}(L_{\text{percent}} \cdot N))\,,$$

where N is the patch vector length. A Hankel trajectory matrix was constructed and its SVD was computed.
7. **Diagonal EWA:** The reconstructed Hankel matrix was transformed back into a time series (image vector) by diagonal averaging, with exponential weighting applied to enhance signal extraction.
8. **Central Pixel Update:** From the reconstructed SSA signal, the value corresponding to the center of the adaptive patch was extracted and assigned to the corresponding pixel of the filtered image.
9. **Iterative Full-Image Reconstruction:** Steps 3-8 were repeated for all pixels until the entire denoised image was constructed.
10. **Quantitative Evaluation:** The denoised image was quantitatively evaluated using PSNR and SSIM to assess the performance of the adaptive PCA–SSA framework.

6 Experimental results of the proposed algorithm

The experimental evaluation conducted on the benchmark images *Lenna* and *Flower*, which were degraded using AGN at noise levels of 10%, 20%, and 30%, demonstrates the effectiveness of the proposed SSA-PCA algorithm. Additive Gaussian noise is modeled as $I_n(x, y) = I(x, y) + n(x, y)$, $n(x, y) \sim \mathcal{N}(\mu, \sigma^2)$, where μ is the mean of the noise (typically zero) and σ is the standard deviation (i.e., the noise intensity). The noise samples are independent and identically distributed across all pixels, meaning that the original image remains unchanged while a random perturbation is added to each pixel. For illustration, consider an 8-bit image with pixel values in the range $0 \leq I(x, y) \leq 255$. A noise level of 10% of the dynamic range corresponds to approximately $\sigma \approx 25$, indicating that each pixel is corrupted by adding a random value drawn from the specified Gaussian distribution. It is important to emphasize that the

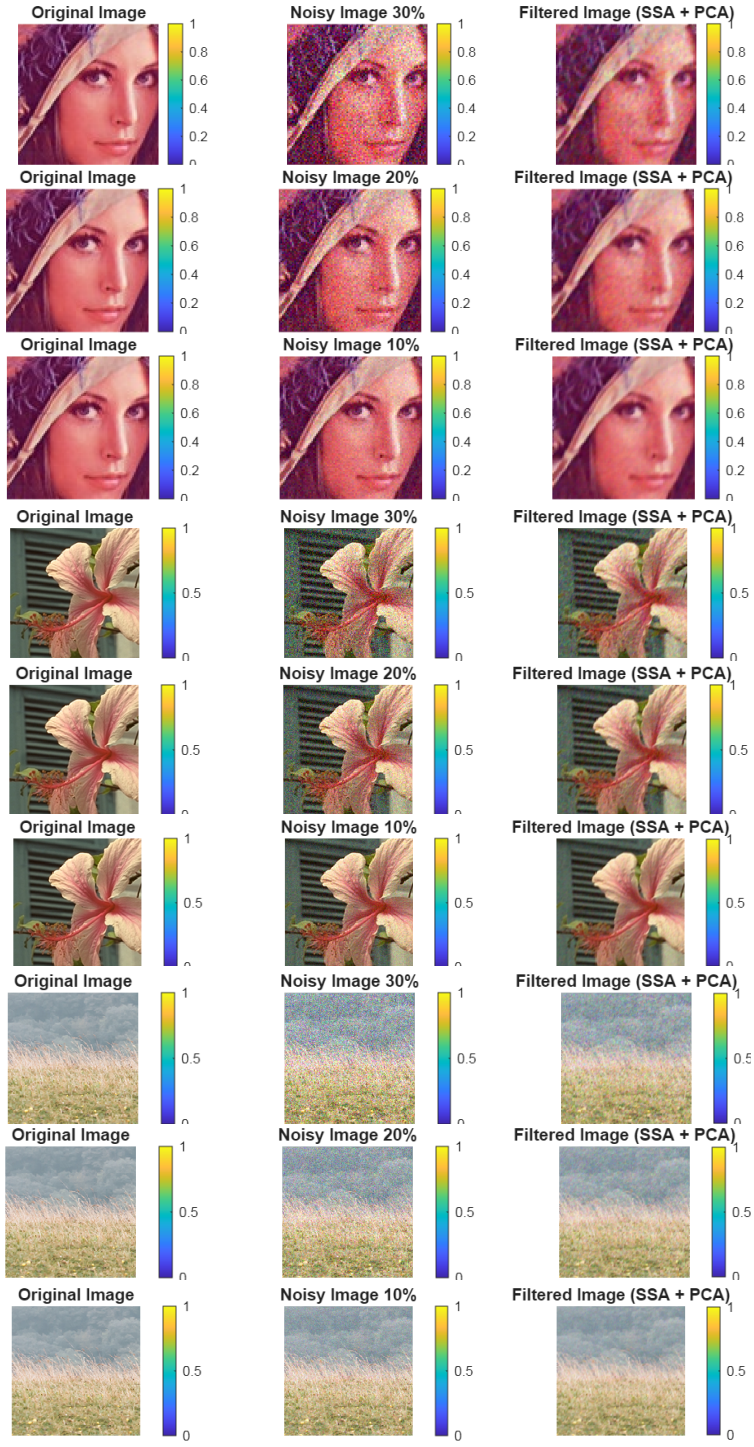

Figure 1: Experimental images “Lenna”, “Flower” and “Horse” under different noise conditions.

original clean images and their Gaussian-degraded versions used in our experiments are exactly aligned with those employed in the studies of Ghasemi and Safariyan (2024) and Latorre-Carmona et al. (2020). This ensures that the observed performance improvements are not due to differences in random noise realization, but rather result from a genuinely superior denoising capability on the same image conditions. By combining local dimensionality reduction through PCA with adaptive reconstruction using SSA, the method achieves noticeable improvements in visual quality compared with conventional denoising approaches.

The quantitative results are presented in Table 1 (PSNR values) and Table **??** (SSIM values). As expected, both indices decrease as the noise level increases, reflecting the typical behavior of denoising algorithms under more challenging conditions. Nevertheless, the proposed model consistently outperforms the PCA-Bootstrap method of Ghasemi and Safariyan (2024) and the EIG method of Latorre-Carmona et al. (2020). For instance, at 30% noise in the *Lenna* image, SSA-PCA achieves 25.70 dB PSNR and 0.9451 SSIM, which are significantly higher than those obtained by the other methods. For the *Flower* image, the improvements are also evident, although the margins are slightly smaller due to its richer textural content. The same consistent behavior is observed in the *Horse* image, where the proposed model maintains a clear advantage across all noise levels. Notably, at 30% noise, SSA-PCA achieves 25.26 dB PSNR and 0.7409 SSIM, while the competing methods experience a substantial performance drop. This demonstrates the robustness of the proposed method in preserving structural information even in images with more complex textures and higher-frequency details.

Table 1: Comparison of denoising performance (PSNR in dB) for “Lenna”, “Flower” and “Horse” images.

	Image	Noise Level	SSA-PCA	PCA-Bootstrap	EIG
PSNR in dB	Lenna	10%	30.54	28.91	29.23
		20%	28.33	26.85	27.14
		30%	25.70	24.12	24.58
	Flower	10%	28.45	27.32	27.65
		20%	26.49	25.18	25.47
		30%	24.86	23.41	23.79
	Horse	10%	32.20	32.18	32.15
		20%	27.33	25.11	24.63
		30%	25.26	20.71	20.22
SSIM	Lenna	10%	0.9812	0.9654	0.9721
		20%	0.9672	0.9487	0.9539
		30%	0.9451	0.9226	0.9315
	Flower	10%	0.9492	0.9328	0.9384
		20%	0.9012	0.8841	0.8927
		30%	0.8427	0.8215	0.8296
	Horse	10%	0.9317	0.9338	0.9321
		20%	0.8290	0.7400	0.7365
		30%	0.7409	0.5528	0.5437

The overall performance trends are illustrated in Figure 2, where PSNR and SSIM values are plotted against noise levels. The results highlight the steady decline of both metrics as noise increases, while consistently confirming the superior performance of

SSA-PCA at each level. Figure 1 provides visual comparisons of the original, noisy, and denoised versions of the *Lenna*, *Flower* and *Horse* images under different noise levels (10%, 20%, and 30%). These visual results confirm that SSA-PCA preserves structural information and image clarity even in high-noise scenarios. Finally, Figure 3 compares the proposed method with PCA-Bootstrap and EIG for the *Lenna*, *Flower* and *Horse* image, demonstrating the superior performance of SSA-PCA, particularly at higher noise levels (20% and 30%).

In summary, the proposed hybrid SSA-PCA model delivers robust denoising performance across all tested conditions. Its advantages are most pronounced in high-noise environments, highlighting its potential for practical applications in real-world image processing tasks.

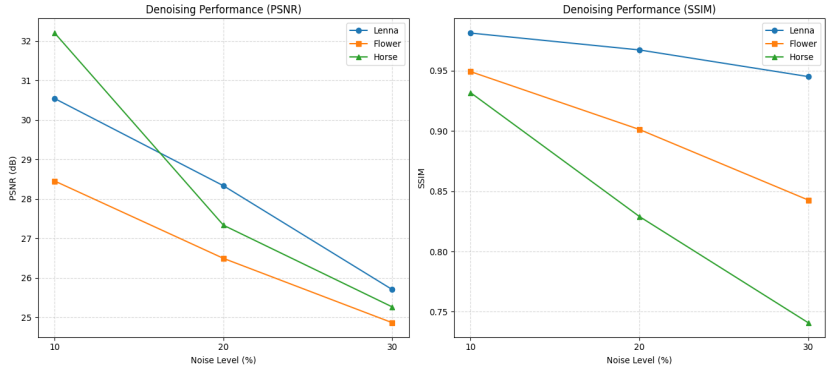

Figure 2: Variation of (a) PSNR and (b) SSIM values with different noise levels for the *Lenna*, *Flower* and *Horse* images using the proposed SSA-PCA method.

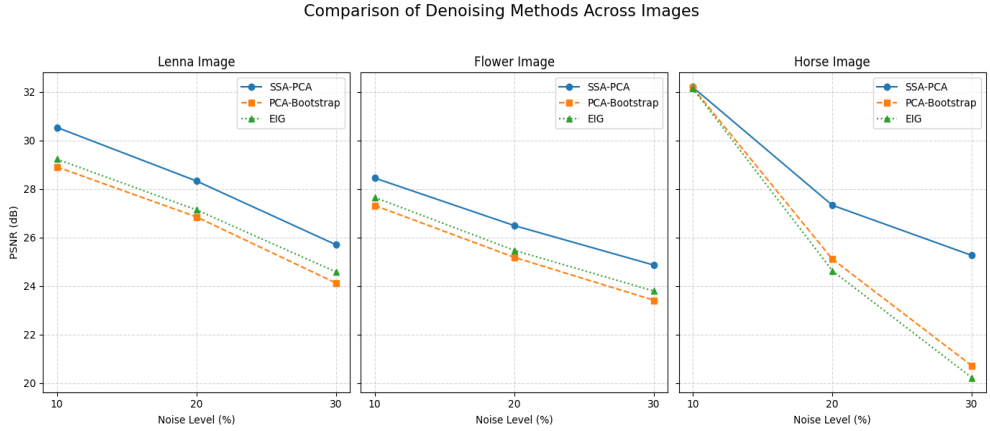

Figure 3: Comparison of PSNR and SSIM indices for the proposed SSA-PCA model, PCA-Bootstrap, and EIG algorithms on the test image *Lenna* ,*Flower* and *Horse*.

7 Conclusion

The problem of noise removal in digital images is of fundamental importance due to its direct impact on visual quality and the performance of subsequent tasks such as image processing, pattern recognition, segmentation, and compression. Nevertheless, the inherent limitations of single-model approaches necessitate the development of hybrid frameworks grounded in solid statistical and mathematical principles. In this regard, the proposed SSA-PCA model was designed to exploit the complementary strengths of two methods. PCA, with its ability to separate the main signal from noise components, and SSA, with its capability to extract trends and hidden patterns in reconstructed data, together provide a statistically stable framework for image denoising. This synergy results in superior preservation of structural details and a substantial reduction in noise levels.

From a quantitative perspective, experimental evaluations on benchmark images such as Lenna and Flower demonstrated that the proposed model achieved significantly higher PSNR and SSIM values compared to PCA-Bootstrap and EIG-based algorithms. Based on the obtained results, it can be concluded that the proposed hybrid model is effective in noise reduction, while also improving PSNR and SSIM, enabling more accurate reconstruction of image structures, and outperforming the existing methods. These findings highlight the necessity of employing hybrid approaches based on statistical and mathematical analyses for image denoising and open new avenues for the development of more advanced algorithms in this field. It is worth noting that the present study specifically addresses additive Gaussian noise (AGN). Consequently, the performance of the proposed SSA-PCA method under other types of noise, or at extremely high noise levels (e.g., above 50%), has not been evaluated. As suggested, future work will consider extending the evaluation to different noise models, including real sensor-dependent noise, and exploring potential enhancements to broaden the applicability of the method in practical image processing tasks.

Acknowledgement

The authors are grateful to the Editor in Chief and referees for the helpful comments and suggestions to improve this manuscript.

References

Buades, A., Coll, B. and Morel, J.M. (2005). A non-local algorithm for image denoising. *IEEE Computer Society Conference on Computer Vision and Pattern Recognition*, **2**:60–65.

Chen, R., Pu, D., Tong, Y. and Wu, M. (2022). Image-denoising algorithm based on improved K-singular value decomposition and atom optimization. *CAAI Transactions on Intelligence Technology*, **7**(1):117–127.

Dabov, K., Foi, A., Katkovnik, V. and Egiazarian, K. (2007). Image denoising by sparse 3-D transform-domain collaborative filtering. *IEEE Transactions on Image Processing*, **16**(8):2080–2095.

Donoho, D.L. and Gavish, M. (2014). The optimal hard threshold for singular values is $4/\sqrt{3}$. *IEEE Transactions on Information Theory*, **60**(8):5040–5053.

Ghasemi, R. (2023). Improving the stability of color image denoising using eigenvector analysis and weighted averaging. *Quarterly Journal of Software Engineering and Intelligent Systems*, **11**(4):22–35.

Ghasemi, R. and Safariyan, A. (2024). Optimal denoising of color images by combining singular-vector analysis and weighted bootstrap sampling. *Third Seminar on Data Science and Its Applications*, Ferdowsi University of Mashhad, 1–9.

Ghasemi, R. and Yousefinejad, M. (2025). An efficient fuzzy filter for impulsive noise reduction in color images. *Journal of Soft Computing and Information Technology*, **14**(1):27–36.

Ghasemi, R., Morillas, S., Nezakati, A. and Rabiei, M. (2022). Image noise reduction by means of bootstrapping-based fuzzy numbers. *Applied Sciences*, **12**(19):9445.

Golyandina, N. and Korobeynikov, A. (2014). *Basic singular spectrum analysis and forecasting with R. Computational Statistics & Data Analysis*, **71**:934–954.

Golyandina, N., Korobeynikov, A. and Zhigljavsky, A. (2018). *Singular Spectrum Analysis with R.* Berlin, Heidelberg: Springer Berlin Heidelberg.

Golyandina, N., Nekrutkin, V. and Zhigljavsky, A. (2001). *Analysis of Time Series Structure: SSA and Related Techniques.* Chapman & Hall/CRC.

Horé, A. and Ziou, D. (2010). Image quality metrics: PSNR vs. SSIM. *20th International Conference on Pattern Recognition*, 2366–2369.

Latorre-Carmona, P., Miñana, J.J. and Morillas, S. (2020). Colour image denoising by eigenvector analysis of neighbourhood colour samples. *Signal, Image and Video Processing*, **14**(3):483–490.

Li, H. and Wu, D. (2025). Hybrid-Domain Synergistic Transformer for Hyperspectral Image Denoising. *Applied Sciences*, **15**(17):9735.

Mafi, M., Martin, H., Cabrerizo, M., Andrian, J., Barreto, A. and Adjouadi, M. (2019). A comprehensive survey on impulse and Gaussian denoising filters for digital images. *Signal Processing*, **157**:236–260.

Momot, A., Spodarev, E. and Zhigljavsky, A. (2005). Bayesian weighted averaging for image denoising. *Mathematical Methods in Applied Sciences*, **28**(14):1761–1776.

Monagi, H. A. and El-Sakka, M.R. (2017). Patch-based models and algorithms for image denoising: a comparative review between patch-based images denoising methods for additive noise reduction. *EURASIP Journal on Image and Video Processing*, **2017**(1):1–22.

Moreno López, M., Frederick, J.M. and Ventura, J. (2021). Evaluation of MRI denoising methods using unsupervised learning. *Frontiers in Artificial Intelligence*, **4**:642731.

Peng, J., Shi, C., Laugeman, E., Hu, W., Zhang, Z., Mutic, S. and Cai, B. (2020). Implementation of the structural similarity (SSIM) index as a quantitative evaluation tool for dose distribution error detection. *Medical Physics*, **47**(4):1907–1919.

Rodríguez-Aragon, L. and Zhigljavsky, A. (2010). Singular spectrum analysis for image processing. *Statistics and Its Interface*, **3**(3):419–426.

Saeedi-Zarandi, M. (2021). A comprehensive review of digital image denoising methods in the transform domain using statistical models and their comparison. *Iranian Journal of Electrical and Computer Engineering*, **18**(1):55–70.

Shakeri, M., Hosseini, S. and Nouri, M. (2019). Noise reduction in cone-beam CT images using independent component analysis. *Iranian Journal of Medical Imaging*, **10**(2):33–45.

Wang, M., Wang, S., Ju, X. and Wang, Y. (2023). Image denoising method relying on iterative adaptive weight-mean filtering. *Symmetry*, **15**(6), 1181.

Yang, M., Wang, H., Hu, K., Yin, G. and Wei, Z. (2022). IA-Net: An inception–attention-module-based network for classifying underwater images. *IEEE Journal of Oceanic Engineering*, **47**(3):704–717.

Zhang, Y., Ding, H., Wang, K. and Li, P. (2023). Hyperspectral image classification based on super pixel-based spatial–spectral PCA fusion, 1D–2D spectral analysis, and random patch network. *Remote Sensing*, **15**(5):1234.

Zou, Y., Yan, C. and Fu, Y. (2023). Iterative denoiser and noise estimator for self-supervised image denoising. In *Proceedings of the IEEE/CVF International Conference on Computer Vision*, 13265–13274.